One-Step Fabrication of Superhydrophobic P(VDF-co-HFP) Nanofibre Membranes Using Electrospinning Technique

Mahmut Tas, Fang Xu, Ifty Ahmed, Xianghui Hou*

Advanced Materials Research Group, Faculty of Engineering, The University of Nottingham, Nottingham, NG7 2RD, UK

Corresponding Author: Dr. Xianghui Hou

E-mail: xianghui.hou@nottingham.ac.uk Tel: +44-115 95 13920

Highlights

- Superhydrophobic surface with low contact angle hysteresis was developed without additional functionalisation and fillers.
- Solvents played the major role of determining the formation of nanofibers and the surface hydrophobicity.
- Superhydrophobicity of the produced membranes was attributed to the specific structures consisting of beads and nanofibers.

Abstract

In this study, superhydrophobic electrospun P(VDF-co-HFP) membranes were fabricated in a one-step electrospinning process. The effects of the key parameters of electrospinning (solution concentration, electrical potential, flow rate and solvent) on the surface roughness, fibre formation and hydrophobicity of the membranes were evaluated using Taguchi method. A 4 x 3 orthogonal array was utilised and the results indicated that the solvent played the critical role in producing the superhydrophobic nanofibre membranes. It was demonstrated that it is possible to produce superhydrophobic membranes with P(VDF-co-HFP) without additional functionalisation and fillers. The highest water contact angle and the lowest contact angle hysteresis obtained were 156° and 5°, respectively, and the roughness values varied from 0.15 to 5.74 μm for the produced P(VDF-co-HFP) nanofibre membranes. The surface superhydrophobicity of the membranes was attributed to the specific structures consisting of a combination of beads and nanofibres.

Key words: Superhydrophobic, electrospinning, nanofibres, fluorinated polymers.

1. INTRODUCTION

Superhydrophobic surface can be defined as a surface which has very high water contact angle (typically >150°) with low contact angle hysteresis (typically <10°) [1]. Due to its non-adhesive and non-wetting characteristics, superhydrophobic surface is critical for many applications such as self-cleaning materials [2], anti-corrosion coatings [3], and low hydrodynamic friction [4, 5], etc. Electrospinning process has been previously utilised to produce superhydrophobic nanofibre membranes [5]. Porous structure and roughness of randomly collected nanofibres contribute to the superhydrophobity of the electrospun membranes. Some of the most popular polymers explored for electrospinning to obtain superhydrophobic surfaces are poly (vinylidene fluoride) [6], poly

(styrene) [7] and poly (sulfone) [8]. However, the hydrophobic behaviour of these polymers is not enough to achieve superhydrophobicity, therefore they were mostly integrated with nanofillers, bead on string structures or via subsequent surface modification techniques. P(VDF-co-HFP) is a copolymer of poly (vinylidene fluoride) and hexafluoropropylene, which has a surface energy of 25 dynes/cm, lower than most of the common polymers [9], such as poly ethylene terephthalate (42 dynes/cm), polystyrene (34 dynes/cm), polyether sulfone (46 dynes/cm), and polyamide 6 (38 dynes/cm). Thus, it is a suitable candidate for producing superhydrophobic surface because of its low surface energy.

Xu *et al.* [10] produced fluorinated polyhedral oligomeric silsesquioxane (POSS) and mixed it with P(VDF-co-HFP) for electrospinning. Two types of fluorinated POSS electrospun nanofibres were collected on glass substrates to obtain transparent superhydrophobic polymeric surfaces. Tijing *et al.* [11] developed P(VDF-co-HFP)/CNT nanocomposite nanofibres to produce superhydrophobic membranes. They reported that the presence of CNTs in/on the nanofibres produced beads on the membrane surface, which increased the overall surface roughness, leading to an increase in water contact angle up to 156°. Shahabadi *et al.* [12] produced nanocomposite fibres using P(VDF-co-HFP) with carbon black to obtain superhydrophobic and superoleophilic membranes with water contact angle, sliding angle and contact angle hysteresis values of 160.8°, 7.0° and 5.3°, respectively. Yoon *et al.* [13] prepared micro/nano-fibrous cellulose triacetate surfaces via electrospinning and then applied plasma treatment using CF_4 precursor. The electrospun membranes without plasma treatment showed a contact angle of 142°, while after CF_4 plasma treatment for 60 seconds a contact angle of 153° was achieved. In another study, Islam *et al*. [14] produced superhydrophobic electrospun membranes from fluorinated silane functionalized pullulan. It was reported that without the functionalisation step using fluorinated silane, it was not possible to directly achieve superhydrophobic pullulan membranes.

Thus far, electrospinning has not been considered as a direct process which provides superhydrophobicity for pure polymers. To achieve superhydrophobicity, it is usually necessary to combine electrospinning with the addition of nanofillers, subsequent surface treatment or functionalization. In this study, superhydrophobic electrospun P(VDF-co-HFP) membranes with low contact angle hysteresis were fabricated directly via a one-step simple process, which were attributed to the specific structures consisting of beads and nanofibres, by varying the electrospinning parameters (i.e. concentration, voltage, solvent and flow rate) without the addition of nanofillers, subsequent surface treatment or functionalization. The work would be useful to guide the fabrication of superhydrophobic nanofibrous membranes. Taguchi method was applied for experimental design and the percentage contribution of each parameter on the surface roughness of the membranes, hydrophobicity, and fibre formation were investigated.

2. EXPERIMENTAL PROCEDURE

2.1 Materials

P(VDF-co-HFP) (average M_W 400.000, average M_n 130.000), dimethylformamide (DMF) (>99%), acetone (>99.9%) and dimethylacetamide (DMAc) (99.8%) were purchased from Sigma Aldrich. All chemicals were used as received, without further purification. The key properties of the solvents are given in Table 1.

Table 1. Some key properties of the solvents used [15-17]

Solvents	Surface Tension (mN/m)	Dielectric Constant	Boiling Point (°C)	Density (g/cm^3)	Vapor Pressure (kPa, at 20°C)
Dimethylacetamide	36.70	37.8	165.1	0.937	0.17
Dimethylformamide	37.10	38.3	153.0	0.994	0.35
Acetone	21.01	27.0	56.0	0.791	24.53

2.2 Design of experiments

L9 Taguchi design which is the most efficient in terms of materials, time and energy consumption, was used for the experimental design. Full factorial design with the four factors: electrical potential, flow rate, concentration and solvent, were considered using three levels per factor. Factors and levels of the Taguchi study employed are given in Table 2 and the nine trial orthogonal arrays explored are listed in Table 3. Furthermore, two productions for each inner array were performed.

Table 2. Factors and levels of Taguchi design

	Factors			
	Concentration (%)	Voltage (kV)	Solvent	Flow Rate (ml/hour)
Levels	10.0	12.5	DMF	1.00
	12.5	17.5	DMAc	1.25
	15.0	22.5	Acetone/DMF	1.50

Table 3. Taguchi orthogonal array with nine trials

Sample Code	Solvent	Concentration (%)	Voltage (kV)	Flow Rate (ml/hour)
DMF-10	DMF	10.00	12.5	1.00
DMAc-10	DMAc	10.00	17.5	1.25
Ac/DMF-10	Acetone/DMF	10.00	22.5	1.50
DMAc-12.5	DMAc	12.50	12.5	1.50
Ac/DMF-12.5	Acetone/DMF	12.50	17.5	1.00
DMF-12.5	DMF	12.50	22.5	1.25
Ac/DMF-15	Acetone/DMF	15.00	12.5	1.25
DMF-15	DMF	15.00	17.5	1.50
DMAc-15	DMAc	15.00	22.5	1.00

2.3 Preparation of P(VDF-co-HFP) solutions

For the preparation of P(VDF-co-HFP) solutions, DMF, DMAc and mixture of DMF and acetone (50/50 wt. %) were used. Various amount of P(VDF-co-HFP) was added to the solvent and mixed using a magnetic stirrer for at least 12 hours at room temperature to obtain clear solutions. After that, 5 ml of solution with three different concentrations (10, 12.5 and 15 wt. % respectively) were loaded in a 10 ml syringe for the electrospinning process.

2.4 Electrospinning process

An in-house electrospinning system with a rotating drum collector was used with low rotation speed (<200 RPM) for the production of random oriented electrospun fibre membranes [18]. Polymer solution containing syringe with a metal needle was mounted on a syringe-pump. The distance between the tip of needle and the collector was kept constant at 15 cm. Flow rate of the polymer solution was chosen as 1, 1.25 and 1.50 ml/h, respectively. Applied voltage was

controlled with a high voltage supplier (Glassman High Voltage Inc. EL series) between 12.5 kV to 22.5 kV. Aluminium foil was used as collector because of its high electrical conductivity and good processability. The set-up of the electrospinning process is shown in Figure 1.

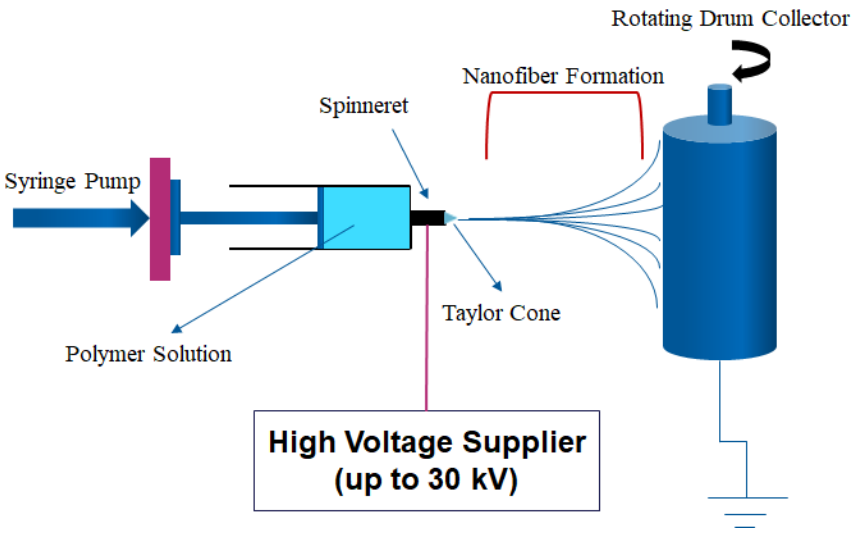

Figure 1. Schematic diagram of the electrospinning process

2.5 Analysing outcomes of the Taguchi method

Signal to noise ratios were calculated using Minitab 17 based on the "larger is better" characteristic formula. To understand the effects of each factor on surface superhydrophobity of electrospun membranes, firstly total variation was calculated using the following formula:

$$S_T = \left[\sum_{i=1}^{N} \bar{Y}_i^2\right] - \left[\frac{\left(\sum_{i=1}^{N} \bar{Y}_i\right)^2}{N}\right] \qquad \text{(Eq. 1)}$$

where Y is the mean water contact angle and *N* is the number of trials in our study. The sum of squares of each factor was also determined with the following formulas:

$$S_A = \frac{A_{10}^2}{3} + \frac{A_{12.5}^2}{3} + \frac{A_{15}^2}{3} - C.F \qquad \text{(Eq. 2)}$$

$$S_B = \frac{B_{12.5}^2}{3} + \frac{B_{17.5}^2}{3} + \frac{B_{22.5}^2}{3} - C.F \quad \text{(Eq. 3)}$$

$$S_C = \frac{C_{DMAc}^2}{3} + \frac{C_{DMF}^2}{3} + \frac{C_{DMF/Acetone}^2}{3} - C.F \quad \text{(Eq. 4)}$$

$$S_D = \frac{D_1^2}{3} + \frac{D_{1.25}^2}{3} + \frac{D_{1.5}^2}{3} - C.F \quad \text{(Eq. 5)}$$

where S is the sum of squares, and A, B, C and D are electrical potential, concentration, flow rate and solvent, respectively. The percentage contribution P_i of each factor was calculated according to Eq. 6.

$$P_i = \frac{S_i}{S_T} \times 100 \quad \text{(Eq. 6)}$$

2.6 Characterisation

Characterisation of the produced nanofibre membranes was conducted by exploring thermal and spectroscopic analyses, morphological characterisation and surface hydrophobicity. Fourier-transform infrared spectroscopy (FT-IR), Raman, differential scanning calorimetry (DSC), thermogravimetric analysis (TGA) and specific heat capacity measurements were conducted. As DMF-10 (shown in Figure 2) demonstrated the highest contact angle, the analysis of material composition and thermal behaviours mainly focused on this sample set.

2.6.1 Morphologic characterisation and surface hydrophobicity

A Joel 7000 scanning electron microscopy (SEM) was used to explore the morphology of the nanofibre membranes with accelerating voltage of 15 kV. A Zeta-20 3D profilometer was used to investigate the surface topography with measuring area of 341 μm x 268 μm. Surface roughnesses were calculated from the area of 200 μm x 0.01 μm. An FTA200 dynamic contact angle system

was used to investigate the surface hydrophobicity of the nanofibre membranes. Static, advancing and receding contact angle were measured and the contact angle hysteresis was calculated using Eq. 7.

$$\theta_{hyst} = \theta_{adv} - \theta_{rec} \qquad \text{(Eq.7)}$$

where θ_{hyst} is contact angle hysteresis, θ_{adv} is the advancing contact angle and θ_{rec} is the receding contact angle.

2.6.2 Thermal and spectroscopic analyses of nanofibre membrane

FT-IR analyse of the produced nanofibre membranes was conducted using a Perkin Elmer FT-IR spectrometer with Attenuated Total Reflection (ATR) between 700 and 3200 cm^{-1}. Raman spectra of the sample were recorded using a Horiba RAMAN spectrometer with 633 nm HeNe laser between 700 and 1500 cm^{-1}.

To determine the thermal properties of the nanofibre membranes, thermogravimetric analysis (TGA, TA Instruments SDT Q600) and Differential scanning calorimetry (DSC, TA instruments DSC2500) analyses were carried out. Specific heat capacity of the nanofibre membrane was also investigated using the TA DSC2500 from 30°C to 110°C.

3. RESULTS AND DISCUSSION

3.1 Morphologic characterisation and surface hydrophobicity

SEM images of the produced nanofibre membranes are shown in Figure 2. Randomly oriented fibres have been obtained without a particular orientation. It was reported that [18], the linear velocity of rotating drum should be greater than 2 m/s to obtain parallel nanofibres. In our study,

the rotation speed of the drum was lower than 200 RPM which equaled to around 0.4 m/s and this value was not sufficient enough to produce oriented nanofibers. It was observed that smooth fibres were formed for Ac/DMF-12.5 and Ac/DMF-15 which used the same solvent; acetone and DMF mixture (50/50 wt. %). DMF-10, Ac/DMF-10, DMF 12.5 and DMF-15 presented a structure consisting of both fibres and beads. They also had much thinner fibre structures compared to other fibrous membranes, with much higher numbers of fibres per unit area. DMF-10, DMAc-10 and Ace/DMF-10 which shared same concentration (10%) did not produce smooth fibres, which may be attributed to the low viscosity of the polymer solutions trialled. It was also observed that when DMAc was used as solvent, the structures obtained were mainly based on a film morphology with limited beads.

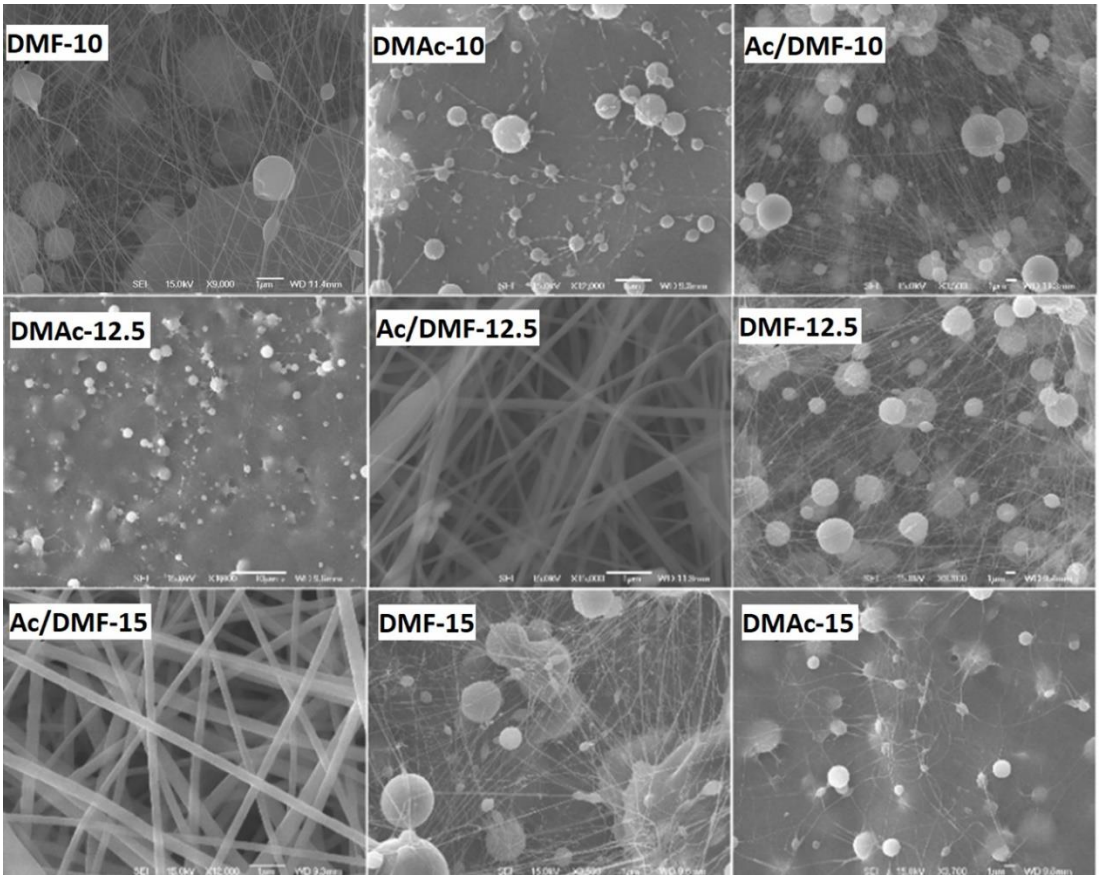

Figure 2. SEM images of the electrospun membranes (see Table 2 for production parameters)

In electrospinning process, viscosity and surface tension of solution are two main parameters of whipping instability which leads to the jet splitting into many small branches [19]. Due to splitting of the jet, much narrower fibres were obtained from the solutions with lower concentration (DMF-10 and Ace/DMF-10) and from the solutions with higher surface tension (DMF-10, DMF-12.5, and DMF-15). However, DMAc-10 was an exception: when DMAc-10 was used as a solvent, solidification step could not be completed and mostly film structures were obtained instead of narrower fibres. It is believed that the main reason is the very low vapour pressure of DMAc (0.17 kPa at 20°C) which limited the evaporation of the solvent during the flight of the jet, between the needle and the collector.

Surface topography has a critical role on surface hydrophobicity. There are some studies which show that increasing roughness leads to the increase in hydrophobicity [20, 21]. The roughness values of the samples produced are given in Figure 3 with topographic images of the highest (a) and the lowest (b) roughness. The lowest roughness (0.15 μm) was taken from DMAc-15 which had a few beads and fibres attached on a film structure, while the highest surface roughness (5.77 μm) was achieved on Ac/DMF-10 which only processed micro-beads structure with fine fibres. It was also clear that the presence of micro beads had a critical effect on roughness. DMF-10, Ac/DMF-10, DMF-12.5 and DMF-15 which had a good mixture of beads with fibres revealed the higher roughness values.

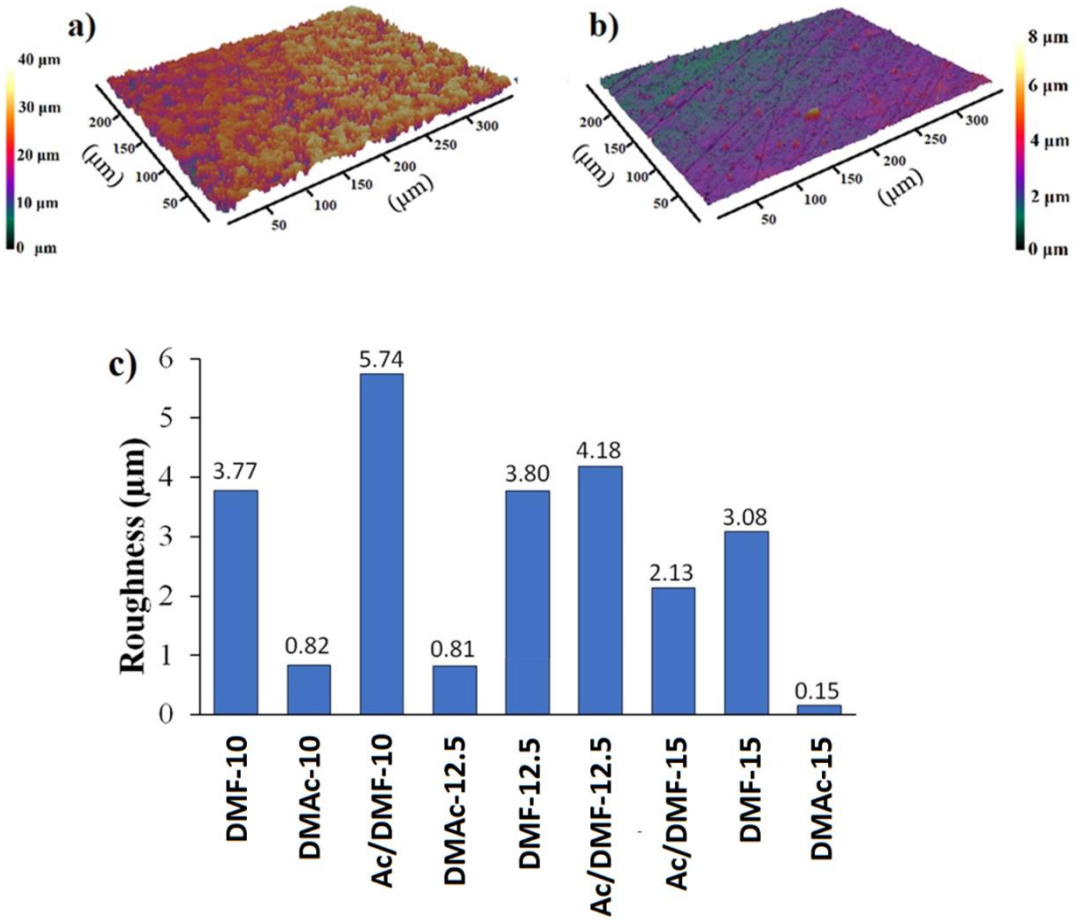

Figure 3. 3D topography of Ac/DMF-10(a) and DMAc-15 (b), Ra roughness values of samples (c)

Static contact angles of the produced samples are shown in Figure 4 (a), together with the roughness values. Samples with low roughness also had low contact angles which were 113°, 112° and 111°, respectively. Contact angles of other samples were higher than 140°, albeit only two of them were considered as superhydrophobic with contact angles of 150.40° and 155.42°. The numbers, size and homogeneity of beads and diameter of the fibres are considered as the two main factors in electrospun membranes which provide higher hydrophobicity. The presence of beads significantly influences the roughness of the membranes. When the roughness increases, effective free energy of the solid/liquid interface also increases, making the surface more hydrophobic [22]. In our study, beads dramatically contributed to the surface roughness, and surfaces with bead and fibre structure provided higher contact angles.

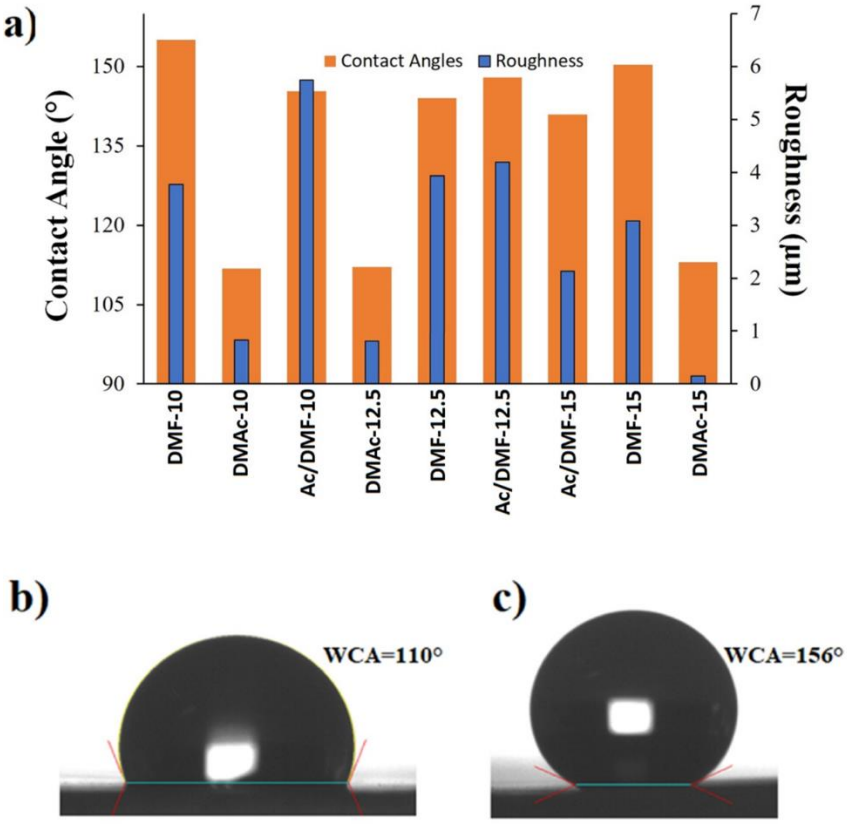

Figure 4. Contact angle and roughness comparison of the produced samples (a), contact angles of DMAc-15 (b) and DMF-10 (c)

The second factor effecting hydrophobicity of the electrospun membrane was the diameter of the fibres. When the fibre diameter decreases, the numbers of the fibres increase, meaning more fibres in a unit area. From SEM analyse, DMF-10, Ac/DMF-10, DMF-12.5 and DMF-15 had much narrower fibres (less than 50 nm) compared to the other fibrous membranes. This structure prevented water droplets from being infused through the gaps, as the fibre diameter decrease and the numbers of fibres increased, the gaps also decreased. Smaller and denser air gaps make hard for the droplets to infuse into the structure, as indicated in Figure 5.

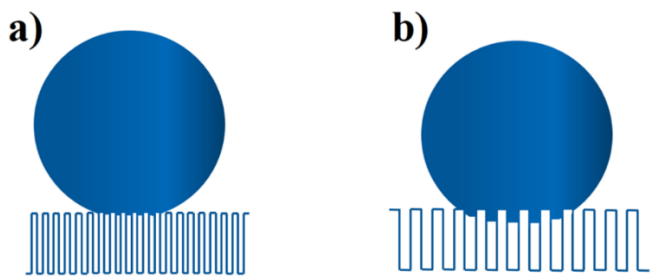

Figure 5. Schematic illustration of the effect of fibre gaps on the contact angle of the electrospun membranes (a) with small gaps and (b) with large gaps

Advancing and receding contact angles of the samples are shown in Figure 6 with values obtained between 1.75 and 6.25 µl sessile volume. It was observed that the highest advancing contact angle was obtained from the sample which had the highest static contact angle. Similar trend was also found on the sample with the lowest advancing contact angle.

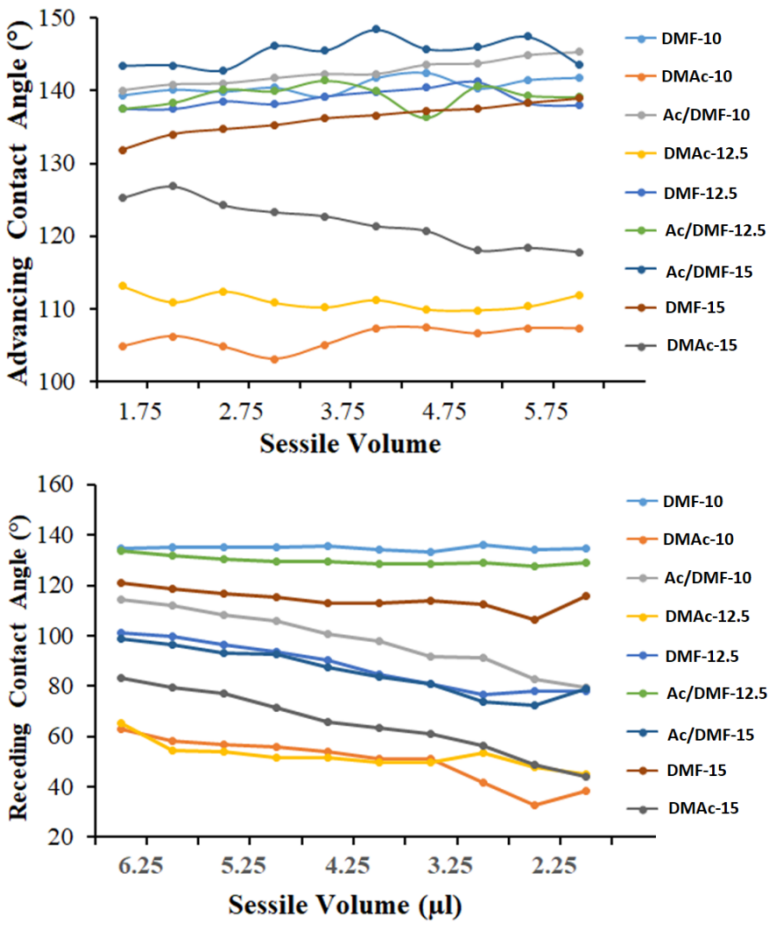

Figure 6. Advancing and receding contact angles of the samples

Contact angle hysteresis (CAH), which is an important indicator of mobility of the droplet on the surface [23], are given in Figure 7. Low CAHs were provided by samples DMF-15, Ac/DMF-12.5 and DMF-10, which also demonstrating high static contact angles. It was also observed that this three samples had stabile CAHs which were not affected by the size of the droplets unlike others.

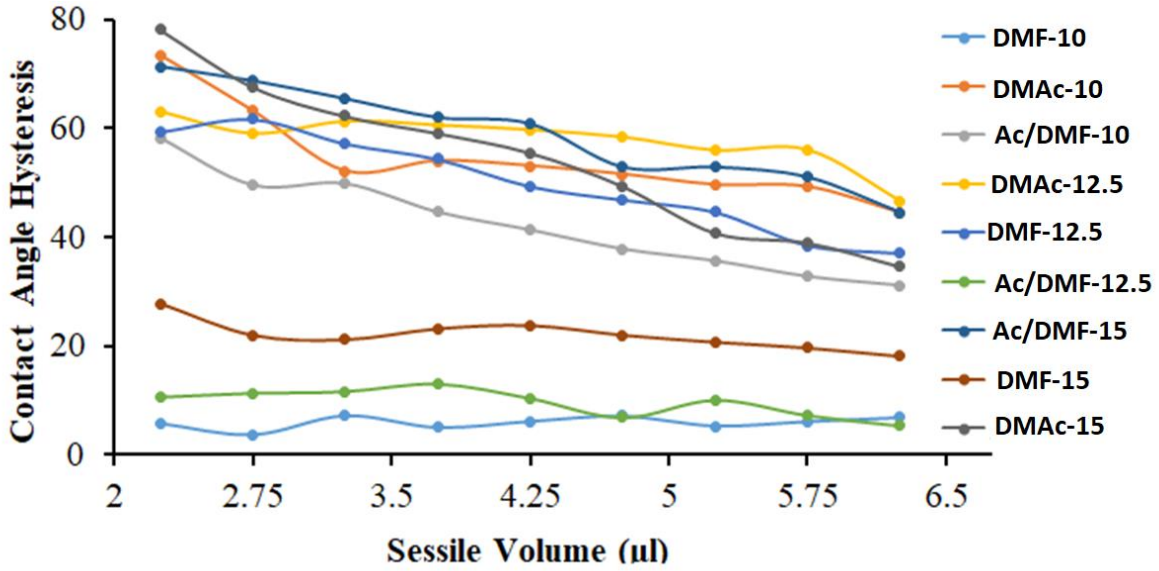

Figure 7. Contact angle hysteresis of the samples

3.2 Thermal and spectroscopic analysis

Raman spectra of the initial polymer and the electrospun membrane are given in Figure 8, in the region between 400 and 1600 cm^{-1}. Characteristic peaks for P(VDF-co-HFP) were detected at 790 cm^{-1} for alpha phase, and 840 cm^{-1} for beta phase for both samples [24] with characteristic CH stretching vibration at 1439 cm^{-1} [25].

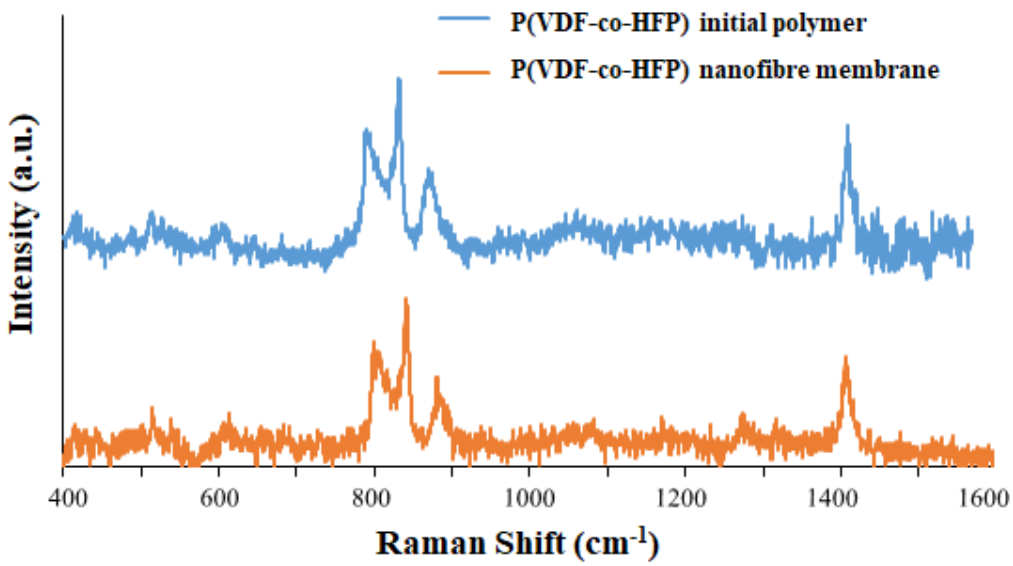

Figure 8. Raman spectra of the electrospun membrane and initial polymer

FT-IR results are shown in Figure 9 in the region between 600 and 3200 cm^{-1}. Asymmetric and symmetric vibration of C-H band were observed at 2987 and 3015 cm^{-1}, respectively. Characteristic absorption peaks of C-F were detected at 1191 and 1405 cm^{-1} [26]. Similar to Raman results, there is no significant change in the FTIR spectra before and after the electrospinning process.

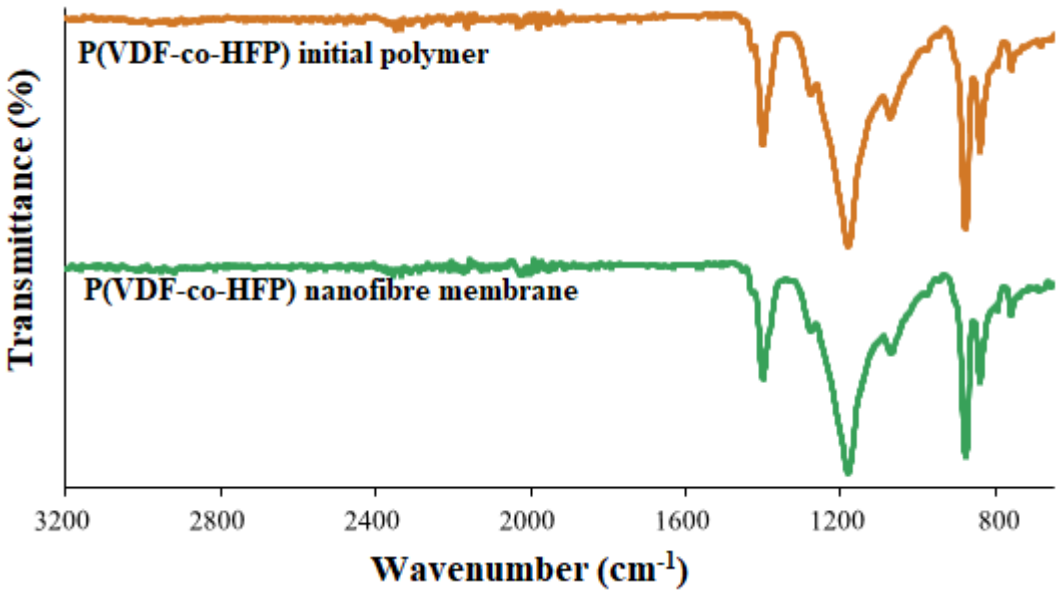

Figure 9. FT-IR spectra of the electrospun membrane and initial polymer

TGA results are given in Figure 10. From the heating curve, there is no significant weight change between 50 and 465°C. It indicates that the thermal decomposition of the superhydrophobic P(VDF-co-HFP) electrospun membrane occurs at around 465 °C under nitrogen. Compared with the raw polymer, there is no obvious change on the decomposition temperature. Residual ash for both samples after 800 °C is approximately 17.5 wt. %.

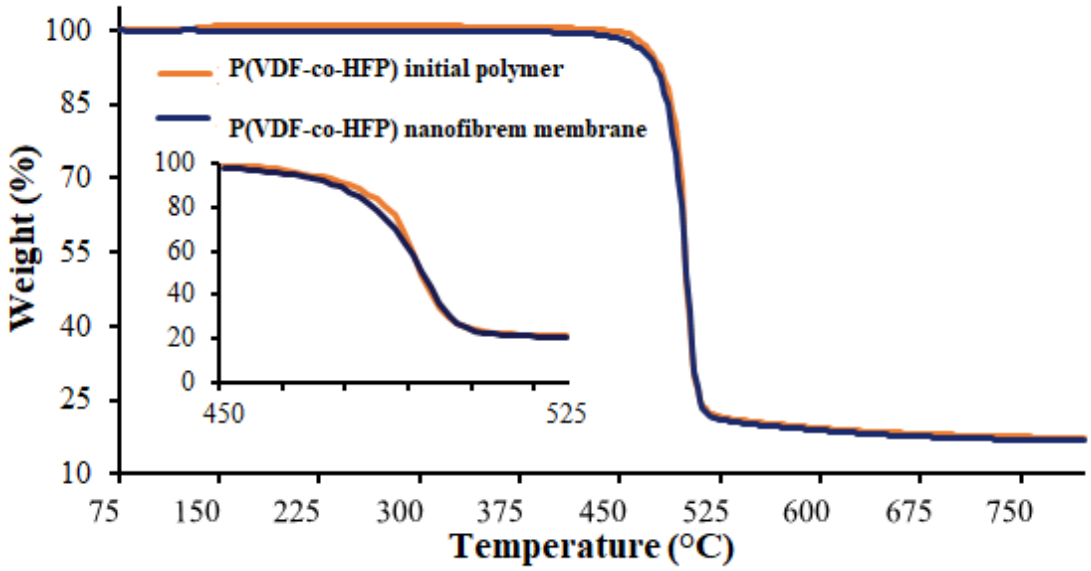

Figure 10. Weight loss (%) versus temperature for nanofibre membrane and initial polymer

The DSC results of the P(VDF-co-HFP) are presented in Figure 11 (endo up). The superhydrophobic electrospun membrane shows an endothermic melting peak at around 146 °C which is only 1°C lower than initial polymer, with a melting enthalpy ($\Delta H_{melting}$) of 26.28 J/g. The crystallinity of the nanofibre membrane is calculated as 25.10%, assuming $\Delta H_{melting}$ 100% crystalline P(VDF-co-HFP) as 104.7 J/g [27]. These results confirm that the process of electrospinning did not significantly affect the melting behaviour of the initial polymer. The small shift from 146°C to 147°C was likely due to the higher surface area of the nanofibre membrane.

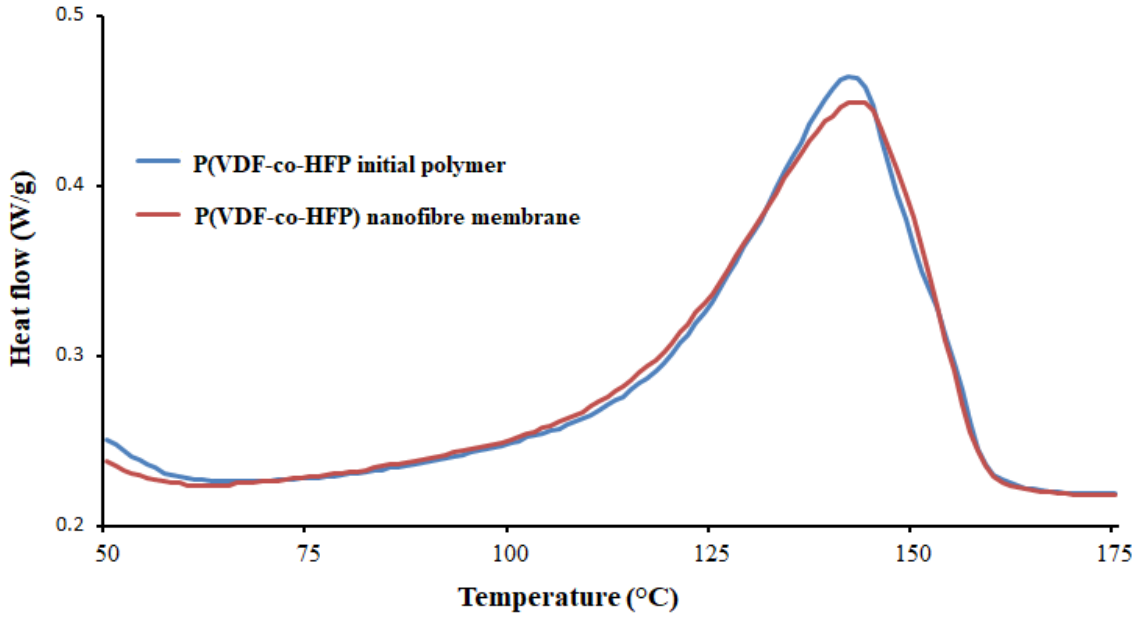

Figure 11. DSC result of the nanofibre membrane and initial polymer

The specific heat capacity of the initial polymer and nanofibre membrane between 30 and 110 °C was shown in Figure 12. As expected, specific heat capacity increases with the increasing temperature. The specific heat capacities of initial polymer and nanofibre membrane are approximately 1.10 J/(g.°C) and 1.16 J/(g.°C) at 30 °C, respectively .

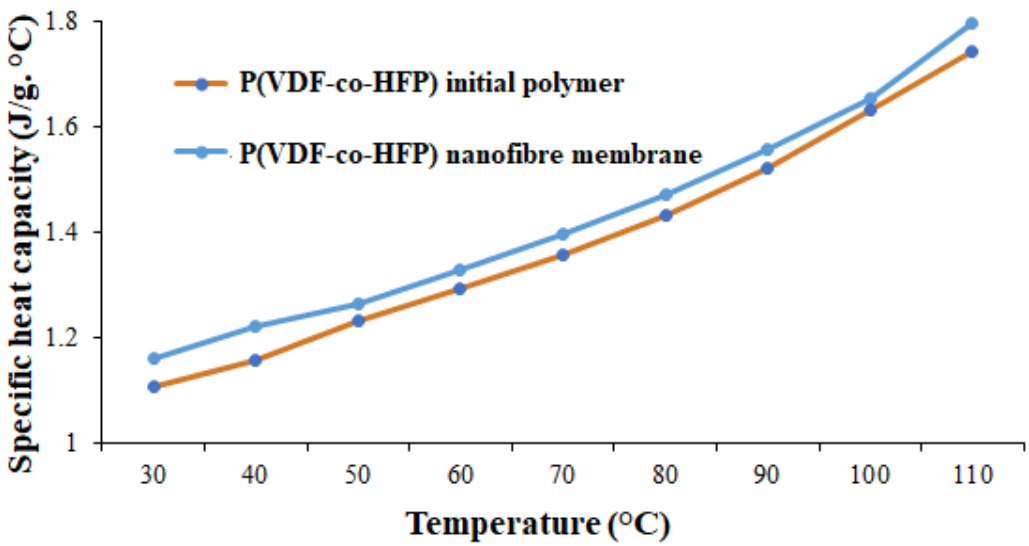

Figure 12. Specific heat capacity of the nanofibre membrane and initial polymer at different temperatures

3.3 Analysis of outcomes from Taguchi method

Plots of signal to noise ratios, which calculated by Minitab 17.2.1 according to the equation of "larger is better", is given in Figure 13. The outcomes are used for the calculation of percentage contribution, which is given in Table 4. Fibre formation is evaluated subjectively with values from 1 (no fibre formation) to 4 (smooth fibre formation) and the signal to noise ratios are calculated according to the given values.

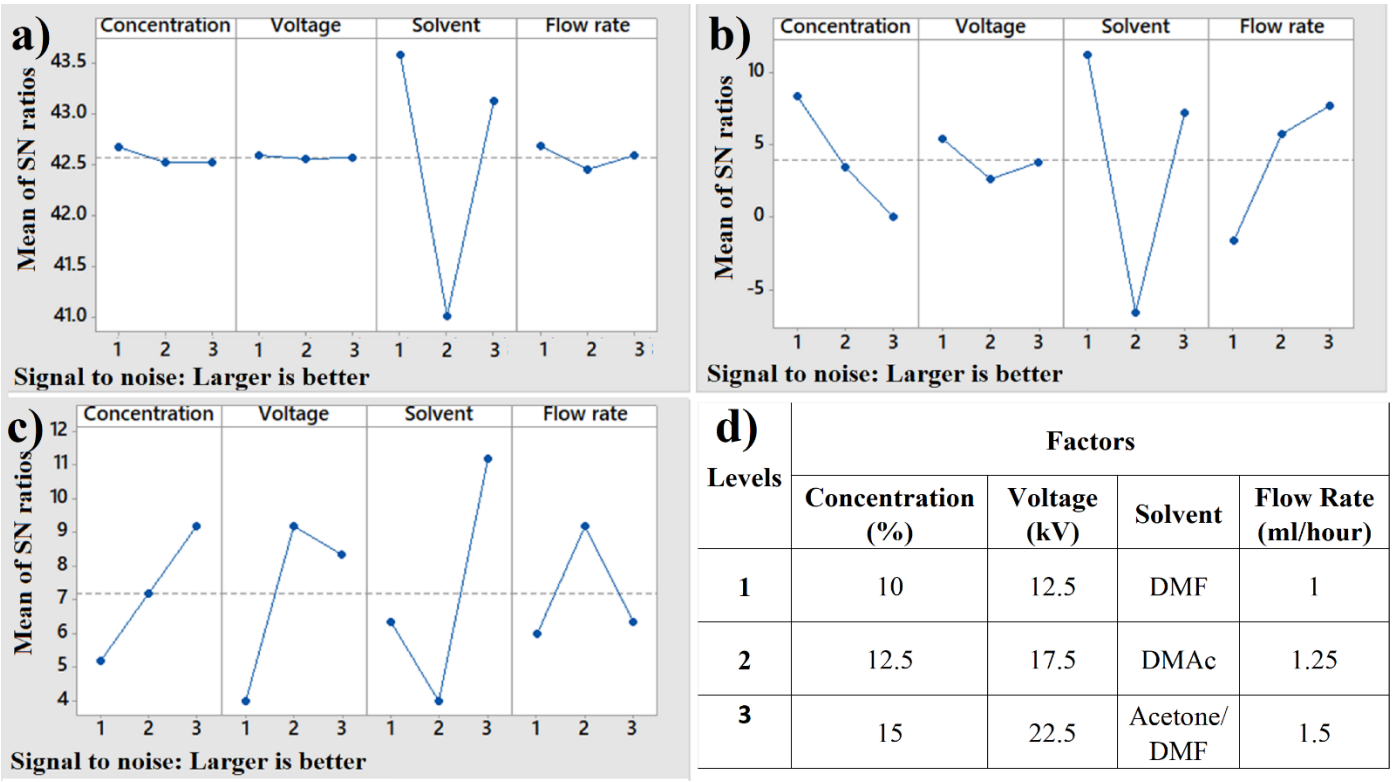

Levels	Factors			
	Concentration (%)	Voltage (kV)	Solvent	Flow Rate (ml/hour)
1	10	12.5	DMF	1
2	12.5	17.5	DMAc	1.25
3	15	22.5	Acetone/ DMF	1.5

Figure 13. Signal-to-noise plots of (a) contact angle, (b) roughness and (c) fibre formation with (d) factors and levels used.

According to the calculation, to achieve higher contact angle, the key parameter suggested was the type of solvent, as its contribution to the contact angle was higher than 98%. The lowest contribution came from DMAc while the highest one was from DMF. The low contribution of DMAc was probably due to its very low volatility and high boiling point. It is reported [16] that

DMAc has 0.17 kPa vapour pressure, which provides longer time for evaporation, compared with DMF which has a much favourable vapour pressure (0.35 kPa) for the formation of fibres. During the electrospinning of DMAc solution, jet formation was observed at the tip of the needle which suggested that the solvent had not completely evaporated between the needle and collector, leading to the non-fibre formation due to the lack of solidification during the flight. The importance of solvents is consistent with reported effects of solvent on the spinnability of polymers, as well as on the morphology evolution and properties of electrospun membranes [28, 29], according to the physicochemical properties of the solvents [21]. Overall, the volatility, dielectric constant, dipole moment, conductivity, density and boiling point, of the solvents may have great influences on the diameter, crystallinity, morphology and spinnability of the fibres [22].

Table 4. Percentage contribution of concentration, voltage, solvent and flow rates

Factors	Contact Angle	Roughness	Fibre Formation
Concentration	0.53	16.99	15.21
Voltage	0.02	15.98	15.21
Solvent	98.6	54.09	60.86
Flow rate	0.83	12.92	8.69

DMF, which is more volatile than DMAc, revealed the highest contribution to the contact angle and roughness. It is believed that solvents with higher surface tension in electrospinning tends to produce some bead structures during fibre formation [30-32]. This is the key reason of why DMF led to the highest contribution to roughness and therefore the hydrophobicity. In our study, beads, which are normally considered as “defects” in electrospinning, are useful for offering improved surface hydrophobicity. DMF has higher surface tension and lower boiling point than DMAc, which led to the formation of both bead and fibre simultaneously. This hybrid structure is ideal for obtaining a superhydrophobic surface.

According to Taguchi calculation, all factors play important roles for the fibre formation. To obtain smooth fibres, DMF/Acetone mixture, which had the lowest surface tension, was an ideal solvent, and increasing concentration also had a positive effect. The flow rate and voltage applied were also critical and there was an optimum point to obtain smooth fibres which was found as 12.5% and 1.25 ml/h respectively.

Table 5. Optimum design of the factors for aimed properties

	Factors			
Aimed Property	Concentration	Voltage	Solvent	Flow Rate
High roughness	10%	12.5 kV	DMF	1.50 ml/h
Smooth fibres	15%	17.5 kV	DMF/Acetone	1.25 ml/h
High contact angle	10%	12.5 kV	DMF	1.0 ml/h

Based on the results above, the specific parameters to obtain nanofibre membranes with the highest roughness, highest contact angle and smooth fibre morphology are summarised in Table 5.

4 CONCLUSIONS

In this study, superhydrophobic P(VDF-co-HFP) membranes were fabricated in a one-step electrospun process. The highest water contact angle and the lowest contact angle hysteresis obtained were 156° and 5°, respectively. The solvent played a critical role in obtaining the surface hydrophobicity of the membranes due to its dominating effect on the morphology of the electrospun membrane, as a result of key properties such as vapour pressure and surface tension, etc. Taguchi method was used to investigate the contribution of key factors on surface roughness, surface hydrophobicity and fibre formation. It was demonstrated that it was possible to produce superhydrophobic P(VDF-co-HFP) membranes with low contact angle hysteresis without any additional functionalization and fillers. The surface superhydrophobicity of the produced membranes was attributed to the specific structures consisting of beads and nanofibres.

Acknowledgement

The authors would like to thank to the Scientific and Technological Research Council of Turkey (TUBITAK), for providing financial support to MAHMUT TAS with the program number 2213, and Nanoscale and Microscale Research Centre (nmRC) at The University of Nottingham for offering access to instrumentation.

References

[1] M. Nosonovsky, B. Bhushan, Superhydrophobic surfaces and emerging applications: Non-adhesion, energy, green engineering. Curr Opin Colloid In, 14 (2009) 270-280.
[2] A. Nakajima, K. Hashimoto, T. Watanabe, K. Takai, G. Yamauchi, A. Fujishima, Transparent superhydrophobic thin films with self-cleaning properties. Langmuir, 16 (2000) 7044-7047.
[3] F.Z. Zhang, L.L. Zhao, H.Y. Chen, S.L. Xu, D.G. Evans, X. Duan, Corrosion resistance of superhydrophobic layered double hydroxide films on aluminum. Angew Chem Int Edit, 47 (2008) 2466-2469.
[4] A.V. Belyaev, O.I. Vinogradova, Hydrodynamic interaction with super-hydrophobic surfaces. Soft Matter, 6 (2010) 4563-4570.
[5] N. Nuraje, W.S. Khan, Y. Lei, M. Ceylan, R. Asmatulu, Superhydrophobic electrospun nanofibers. J Mater Chem A, 1 (2013) 1929-1946.
[6] Z.P. Zhou, X.F. Wu, Electrospinning superhydrophobic-superoleophilic fibrous PVDF membranes for high-efficiency water-oil separation. Mater Lett, 160 (2015) 423-427.
[7] B.D.B. Tiu, H.N. Nguyen, D.F. Rodrigues, R.C. Advincula, Electrospinning Superhydrophobic and Antibacterial PS/MWNT Nanofibers onto Multilayer Gas Barrier Films. Macromol Symp, 374 (2017) 1600138.
[8] M. Al-Qadhi, N. Merah, A. Matin, N. Abu-Dheir, M. Khaled, K. Youcef-Toumi, Preparation of superhydrophobic and self-cleaning polysulfone non-wovens by electrospinning: influence of process parameters on morphology and hydrophobicity. J Polym Res, 22 (2015) 844.
[9] K.L. Mittal, Contact Angle, Wettability and Adhesion, Volume 4, CRC Press, 2006.
[10] V.A. Ganesh, A.S. Nair, H.K. Raut, T.T.Y. Tan, C.B. He, S. Ramakrishna, J.W. Xu, Superhydrophobic fluorinated POSS-PVDF-HFP nanocomposite coating on glass by electrospinning. J Mater Chem, 22 (2012) 18479-18485.
[11] L.D. Tijing, Y.C. Woo, W.G. Shim, T. He, J.S. Choi, S.H. Kim, H.K. Shon, Superhydrophobic nanofiber membrane containing carbon nanotubes for high-performance direct contact membrane distillation. J Membrane Sci, 502 (2016) 158-170.
[12] S.M.S. Shahabadi, J.A. Brant, Bio-inspired superhydrophobic and superoleophilic nanofibrous membranes for non-aqueous solvent and oil separation from water. Sep Purif Technol, 210 (2019) 587-599.
[13] Y. Il Yoon, H.S. Moon, W.S. Lyoo, T.S. Lee, W.H. Park, Superhydrophobicity of PHBV fibrous surface with bead-on-string structure. J Colloid Interf Sci, 320 (2008) 91-95.

[14] M.S. Islam, N. Akter, M.R. Karim, Preparation of superhydrophobic membranes by electrospinning of fluorinated silane functionalized pullulan. Colloid Surface A, 362 (2010) 117-120.
[15] A. Celebioglu, T. Uyar, Electrospun porous cellulose acetate fibers from volatile solvent mixture. Mater Lett, 65 (2011) 2291-2294.
[16] S. Wu, Q. Burlingame, Z.X. Cheng, M.R. Lin, Q.M. Zhang, Strongly Dipolar Polythiourea and Polyurea Dielectrics with High Electrical Breakdown, Low Loss, and High Electrical Energy Density. J Electron Mater, 43 (2014) 4548-4551.
[17] K. Yoon, B.S. Hsiao, B. Chu, Formation of functional polyethersulfone electrospun membrane for water purification by mixed solvent and oxidation processes. Polymer, 50 (2009) 2893-2899.
[18] Y.Z. Long, M. Yu, B. Sun, C.Z. Gu, Z.Y. Fan, Recent advances in large-scale assembly of semiconducting inorganic nanowires and nanofibers for electronics, sensors and photovoltaics. Chem Soc Rev, 41 (2012) 4560-4580.
[19] H. Zhao, H. Chi, Electrospun Bead-on-String Fibers: Useless or Something of Value? Novel Aspects of Nanofibers, (2018) 87-102.
[20] I. Hejazi, J. Seyfi, G.M.M. Sadeghi, S.H. Jafari, H.A. Khonakdar, A. Drechsler, S.M. Davachi, Investigating the interrelationship of superhydrophobicity with surface morphology, topography and chemical composition in spray-coated polyurethane/silica nanocomposites. Polymer, 128 (2017) 108-118.
[21] A. Davis, Y.H. Yeong, A. Steele, I.S. Bayer, E. Loth, Superhydrophobic Nanocomposite Surface Topography and Ice Adhesion. Acs Appl Mater Inter, 6 (2014) 9272-9279.
[22] C. Yang, U. Tartaglino, B.N.J. Persson, Influence of surface roughness on superhydrophobicity. Phys Rev Lett, 97 (2006) 116103.
[23] Y.H. Xiu, L.B. Zhu, D.W. Hess, C.P. Wong, Relationship between work of adhesion and contact angle hysteresis on superhydrophobic surfaces. J Phys Chem C, 112 (2008) 11403-11407.
[24] M.T. Riosbaas, K.J. Loh, G. O'Bryan, B.R. Loyola, In Situ Phase Change Characterization of PVDF Thin Films using Raman Spectroscopy. Sensors and Smart Structures Technologies for Civil, Mechanical, and Aerospace Systems 2014, (2014) 9061.
[25] Y.L. Ji, J. Liu, Y.J. Jiang, Y.L. Liu, Analysis of Raman and infrared spectra of poly (vinylidene fluoride) irradiated by KrF excimer laser. Spectrochim Acta A, 70 (2008) 297-300.
[26] Y. Bormashenko, R. Pogreb, O. Stanevsky, E. Bormashenko, Vibrational spectrum of PVDF and its interpretation. Polym Test, 23 (2004) 791-796.
[27] U.R. Farooqui, A.L. Ahmad, N.A. Hamid, Effect of polyaniline (PANI) on Poly(vinylidene fluoride-co-hexaflouro propylene) (PVDF-co-HFP) polymer electrolyte membrane prepared by breath figure method. Polym Test, 60 (2017) 124-131.
[28] J. Lasprilla-Botero, M. Alvarez-Lainez, J.M. Lagaron, The influence of electrospinning parameters and solvent selection on the morphology and diameter of polyimide nanofibers. Mater Today Commun, 14 (2018) 1-9.
[29] Z. Song, S.W. Chiang, X.D. Chu, H.D. Du, J. Li, L. Gan, C.J. Xu, Y.W. Yao, Y.B. He, B.H. Li, F.Y. Kang, Effects of solvent on structures and properties of electrospun poly(ethylene oxide) nanofibers. Journal of Applied Polymer Science, 135 (2018) 45787.
[30] A. Haider, S. Haider, I.K. Kang, A comprehensive review summarizing the effect of electrospinning parameters and potential applications of nanofibers in biomedical and biotechnology. Arab J Chem, 11 (2018) 1165-1188.
[31] D.H. Reneker, A.L. Yarin, Electrospinning jets and polymer nanofibers. Polymer, 49 (2008) 2387-2425.
[32] S.Q. Huan, G.X. Liu, G.P. Han, W.L. Cheng, Z.Y. Fu, Q.L. Wu, Q.W. Wang, Effect of Experimental Parameters on Morphological, Mechanical and Hydrophobic Properties of Electrospun Polystyrene Fibers. Materials, 8 (2015) 2718-2734.